

Two-photon imaging of spatially extended neuronal network dynamics with high temporal resolution

Kyle P. Lillis^{a,b,c}, Alfred Eng^a, John A. White^{a,b,c,d}, Jerome Mertz^{a,*}

^a Department of Biomedical Engineering, Boston University, Boston, MA 02215, United States

^b Center for BioDynamics, Boston University, Boston, MA, United States

^c Center for Memory and Brain, Boston University, Boston, MA 02215, United States

^d Department of Bioengineering, University of Utah, Salt Lake City, 84112 UT, United States

ARTICLE INFO

Article history:

Received 24 January 2008

Received in revised form 13 March 2008

Accepted 17 April 2008

Keywords:

Calcium imaging

Laser scanning

Epileptiform

Spatiotemporal

ABSTRACT

We describe a simple two-photon fluorescence imaging strategy, called targeted path scanning (TPS), to monitor the dynamics of spatially extended neuronal networks with high spatiotemporal resolution. Our strategy combines the advantages of mirror-based scanning, minimized dead time, ease of implementation, and compatibility with high-resolution low-magnification objectives. To demonstrate the performance of TPS, we monitor the calcium dynamics distributed across an entire juvenile rat hippocampus (>1.5 mm), at scan rates of 100 Hz, with single cell resolution and single action potential sensitivity. Our strategy for fast, efficient two-photon microscopy over spatially extended regions provides a particularly attractive solution for monitoring neuronal population activity in thick tissue, without sacrificing the signal-to-noise ratio or high spatial resolution associated with standard two-photon microscopy. Finally, we provide the code to make our technique generally available.

© 2008 Elsevier B.V. All rights reserved.

1. Introduction

There has been a recent trend toward applying two-photon microscopy to image the activity of neuronal populations rather than individual neurons. However, because two-photon microscopy requires laser scanning, such imaging invariably involves a tradeoff between temporal resolution and field of view, or FOV (i.e. the spatial extent of the region accessible by the laser focal spot).

By far, the most widely used scanning mechanism for two-photon microscopy makes use of mirrors mounted on galvanometers. Mirrors have the advantage that they can handle high powers, provoke essentially no power loss, are equally efficient for a wide range of tilt angles, and are achromatic. However, the drawback of galvanometers is that they can be quite slow when used in a conventional raster-scanning mode, typically requiring about a second to perform an x - y scan over the full microscope FOV. Several strategies have been adopted to improve image acquisition speed. For example, fast multi-photon imaging has been achieved by splitting the beam and scanning the sample with multiple beamlets (Bewersdorf et al., 1998; Kurtz et al., 2006). However, because

two-photon microscopy is based on nonlinear excitation, the redistribution of laser power into multiple lower-power beamlets leads to a reduction in fluorescence power. Such a strategy also requires an imaging of fluorescence signal with an array detector, largely undermining the main advantage of two-photon microscopy when imaging in thick tissue (Helmchen and Denk, 2005).

Alternatively, fast single-beam scanning has been achieved with the use of resonant scanners (Fan et al., 1999) or rotating polygonal mirrors (Kim et al., 1999), though with the constraint of fixed raster-scan patterns. Recently, a spiral-scan strategy coupled with an oscillating focus has provided a remarkable 10 Hz scan rate over a $250 \mu\text{m} \times 250 \mu\text{m} \times 250 \mu\text{m}$ 3D volume (Göbel et al., 2007). Such strategies are highly effective for dense cell populations and indeed have been used to image hundreds of cells in a single scan. However, these strategies become less effective when the cells of interest are sparsely distributed because of their inefficient use of scan time: the laser beam spends little useful time illuminating the cells of interest while spending much dead time illuminating regions around these cells.

An alternative strategy to reduce dead time is the random-access approach where the laser focus is aimed only at specific cells of interest. This strategy has been adopted with two-photon microscopes based on acousto-optic deflectors (AOD's), the advantage being that AOD's are fast because they are inherently inertia-free (Iyer et al., 2006; Lechleiter et al., 2002; Roorda et al., 2004). However, AOD's impose their own constraints. Because their scan

* Corresponding author. Tel.: +1 617 358 0746; fax: +1 617 358 4216.
E-mail address: jmertz@bu.edu (J. Mertz).

angles are much smaller than galvanometer's, they offer significantly reduced FOV's for a given microscope objective. Moreover, their transmission efficiencies are angle dependent and their chromatic dispersion leads to degraded resolution, which can only be partially corrected with complicated techniques of dispersion compensation (Lechleiter et al., 2002; Roorda et al., 2004; Salomé et al., 2006).

We provide the details here of a simple strategy, called targeted path scanning (TPS), which is an extension of a previously reported vector-mode approach (Nikolenko et al., 2007) that combines the advantages of mirror-based scanning and random-access targeting. Our strategy can readily be implemented using the hardware of standard two-photon microscopes, maintains a constant user-prescribed sampling rate and pixel size within cells of interest, and minimizes dead time between cells of interest. We demonstrate neuronal network activity measurements at 100 Hz scan rates over spatial ranges in the millimeter range, without sacrificing either the spatial resolution or the signal-to-noise ratio (SNR) associated with standard two-photon microscopy.

2. Materials and methods

2.1. Electrophysiological recordings and staining

All protocols were approved by the Boston University Animal Care and Use Committee. Transverse hippocampal brain slices (400 μm) were prepared as previously described (Netoff et al., 2005) from Long-Evans rats aged P14–32. After a 1-h incubation period, they were transferred to the recording chamber. Slices were initially visualized using graded-field microscopy (Yi et al., 2006). The areas of interest were then stained with Calcium Green-1 AM (Invitrogen, Carlsbad, CA) using multicell bolus loading (but cf. Garaschuk et al., 2006; Stosiek et al., 2003), in which a Picospritzer II (Parker Hannifin, Pine Brook, NJ) is used to inject dye through a glass pipette (3–6 $\text{M}\Omega$ when filled with KCl-based dye solution) directly into the brain tissue. We note that while Calcium Green-1 remains fluorescent in the absence of calcium, many dyes (e.g. Calcium Green-2) lose their fluorescence altogether. Because the imaging technique described here depends on selecting cells from images of a resting slice, it is important to either use a dye that is fluorescent in resting cells or to perform a dual stain with a morphological dye (such as Calcein Orange AM). Either a field potential recording (<1 $\text{M}\Omega$, filled with, in mM, 126 NaCl, 2.5 KCl, 1.25 NaH_2PO_4 , 2 MgCl_2 , 26 NaHCO_3 , 25 dextrose, 2 mM CaCl_2) or a whole-cell patch clamp recording (3–6 $\text{M}\Omega$, filled with 120 mM potassium gluconate, 10 mM KCl, 10 mM HEPES, 4 mM Mg-ATP, 0.3 mM Tris-GTP, 10 mM sodium phosphocreatine, 20 units/ml creatine kinase and 10 μM Calcium Green-1 hexapotassium salt) was acquired simultaneously from the region being imaged. All electrophysiological recordings were obtained with a Multiclamp 700B (Axon Instruments, Foster City, CA). For cell-attached recordings, the dye was omitted from the intracellular solution to eliminate any possibility of elevating dye concentration above that achieved with bulk-loading. An extracellular stimulation electrode was placed near the cell being recorded during the cell-attached patch experiments.

2.2. Targeted path scanning

All imaging was performed using a custom-built two-photon microscope based on a Ti-Sapphire mode-locked laser source operating at 810 nm, 80 MHz repetition rate, and ~ 100 fs pulse-width (Tsunami and Millennia V, Spectra Physics, Mountain View, CA), equipped with x - y galvanometer-mounted mirrors (VM500 scanners with 4-mm mirrors, driven by MiniSax servo amplifiers, GSI

Lumonics, Billerica, MA), and controlled by custom Labview software and a PCI-6251 data acquisition board (National Instruments, Austin, TX). Images were acquired using a 60×0.9 NA, 10×0.3 NA, or a 20×0.95 NA water immersion objective (Olympus, Tokyo, Japan). To avoid imaging neuropil above or below the region of interest, it is important to consider the optical axial resolution (Zipfel et al., 2003) and the axial size of the regions of interest. Assuming objects selected are roughly centered near the plane of focus, the axial resolution should ideally be chosen to be smaller than the axial size of the regions of interest. In the examples shown here (somata of pyramidal neurons, radius ≈ 10 μm), the $20\times$ objective (0.95 NA) easily provides sufficient axial resolution to ensure that signal originates from the intended ROI, while the $10\times$ objective (0.3 NA) just meets the above criterion.

The system is capable of collecting fluorescent light both above and below the sample simultaneously to improve the signal-to-noise ratio. However, to demonstrate the SNR obtained in the most widely used configuration (epifluorescence), all data shown here were collected from above the sample (i.e. through the objective) only.

After a dye incubation period of ~ 1 h, a high-resolution two-dimensional image of the full FOV was acquired by standard raster scan and displayed on the computer screen. The user then selected various regions of interest (e.g. cell somas) from the two-dimensional image. Specifically, the user clicked, with a mouse, on two points defining the entrance and exit of each region of interest, thereby defining segments of interest (SOI's) through each region. This process was repeated for each SOI. A closed-loop path including each SOI (in the order they were selected) was then automatically generated (Fig. 1A). TPS then consisted in repeatedly scanning the laser beam along this path. The detection sampling rate was held constant at either 100 or 125 kHz (respectively corresponding to a fixed integration time of 10 μs or 7 μs). However, the scan velocity was varied along the path so as to maintain adequate SNR while minimizing dead time. Specifically, the user-defined SOI's along the path were scanned with a fixed velocity that was adjusted to ensure enough time for adequate signal accumulation per SOI, whereas the scan velocity spent between these SOI's was subjected to what is known as "bang-bang" control: maximal acceleration followed by maximal deceleration (Fig. 1B–C; note: the sample points are unevenly spaced along the scan path). For more specific details, and to make our technique generally available, we have included LabVIEW and Matlab code in the Supplemental methods to demonstrate the scan-path generation algorithm.

Finally, data were recorded in y - t plots (Fig. 3B) where the y -axis corresponds to the unwrapped position along the scan path, and a row corresponds to the temporal fluorescence activity monitored at a given point in space over the total duration of the recording. To maximize SNR, traces of the activity associated with each SOI were obtained by averaging the rows encompassing each SOI, and displayed as relative fluorescence $\Delta F/F$ (Fig. 3C). Unless otherwise noted, fluorescent traces shown are low-pass filtered at 10 Hz.

3. Results

TPS relies on steering the laser beam along a well-defined path. To evaluate the speed at which the galvanometers can accurately track this path, we tested TPS with a worst-case-scenario scan path where three SOI's were separated by a large distance. The actual position of the galvanometer, provided by the galvanometer control electronics, was recorded for different values of maximal intercellular acceleration (i.e. for different scan rates). Although it was possible to intersect regions of interest the size of a pyramidal neuron soma at a scan rate of 397 Hz (Fig. 2), the number of

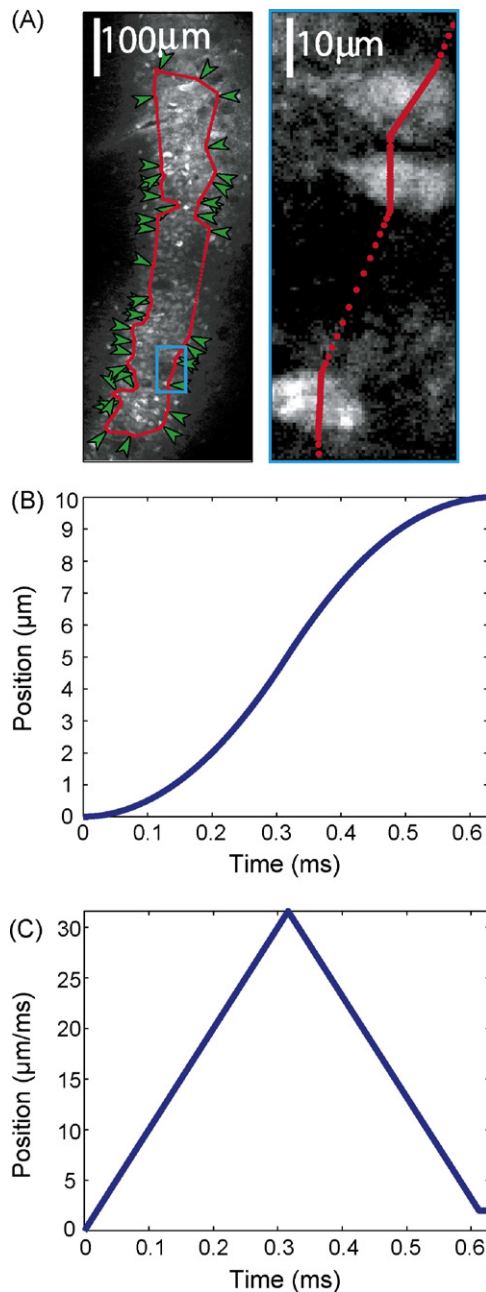


Fig. 1. Generation of laser trajectory. (A) The user specifies a path for the laser beam by pairwise selecting points that define segments through each region of interest (ROI) in a 2D image (of CA1 in this example). ROIs (inset) are sampled at a constant velocity, while the intervals between ROIs are traversed using maximal acceleration and deceleration. Red dots represent samples collected; every third is shown. A bang-bang control scheme was used to generate the laser trajectory between regions of interest. The implementation of this control system involved maximally accelerating the galvanometers until the halfway point between the ROIs, then decelerating maximally. To avoid an unnecessarily slow approach to the ROI, the galvanometers were not decelerated below a user-specified minimum velocity. This produced (B), a sigmoidal position profile and (C), a triangular velocity profile (until the fixed, minimal velocity segment near the end). The maximal acceleration specified for the simulation shown here was arbitrarily chosen to be $100 \mu\text{m}/\text{s}^2$.

samples recorded from the region became reduced, effectively curtailing the prescribed residence time within the region. To ensure that the specified residence time was roughly maintained, the maximal galvanometer acceleration was capped at a level that resulted in a scan rate of 110 Hz for the test path shown in Fig. 2 ($1.84 \times 10^6 \text{ degrees}/\text{s}^2$). The corresponding acceleration (\ddot{x}) of the

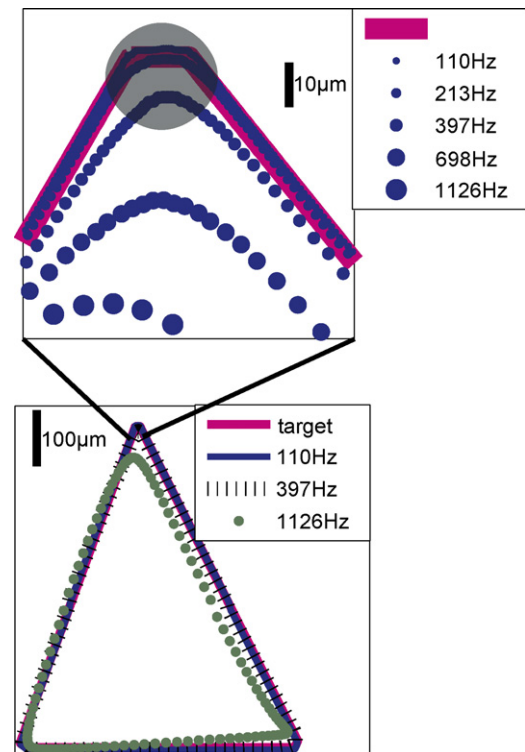


Fig. 2. Evaluation of scan-path accuracy using position output from the galvanometer. A challenging path, a triangle of ROIs separated by 600–700 μm , was chosen to evaluate the tradeoff between position accuracy and scan rate. The actual position of the laser as measured using the measured position output from the galvanometer controller (blue dotted lines) was compared to the target path (pink solid line) at five different maximum intercellular acceleration rates (resulting in the five different round-trip “scan rates” listed in the legend). For scan rates up to ~ 400 Hz the laser remained within a region approximately the size of a pyramidal neuron soma (depicted as a gray disk).

laser spot in the sample depends on the beam expansion factor (E) and the focal length of the objective (f) according to:

$$\ddot{x} \simeq \frac{f\ddot{\theta}}{E} \quad (1)$$

(We note that for the Olympus objectives used here $f = 180 \text{ mm}/M$ where M is the objective magnification.) The same maximal angular acceleration, derived from the worst-case-scenario described above, was used for the collection of all subsequent data. Because the sampling frequency is fixed (100 kHz or 125 kHz) the overall scan period is directly proportional to the number of samples in the selected scan path. For the examples shown here, a fixed within-cell sample spacing of $0.16 \mu\text{m}/\text{sample}$, approximately 40 samples (pixels) per cell were collected along each line segment of interest defined by the user. With the fixed intercellular acceleration and intracellular velocity, the scan rate depends only on the number of cells selected and the distances between them. We note that more complex galvanometer control schemes (e.g. Tan et al., 1999) could be implemented to provide somewhat better scan-path tracking around sharp corners, however, we found that these schemes were not needed to attain suitable scan speed and accuracy for imaging at the cellular level.

To demonstrate the capability of TPS to monitor spatiotemporal firing patterns, 4-aminopyridine was added to the bath to induce epileptiform activity (Chesnut and Swann, 1988; Perreault and Avoli, 1989). Forty-one cells distributed over an area of $1.6 \text{ mm} \times 1.8 \text{ mm}$ were imaged at a scan rate of 31 Hz (Fig. 3A). Both seizure-like events and interictal bursting were apparent in many

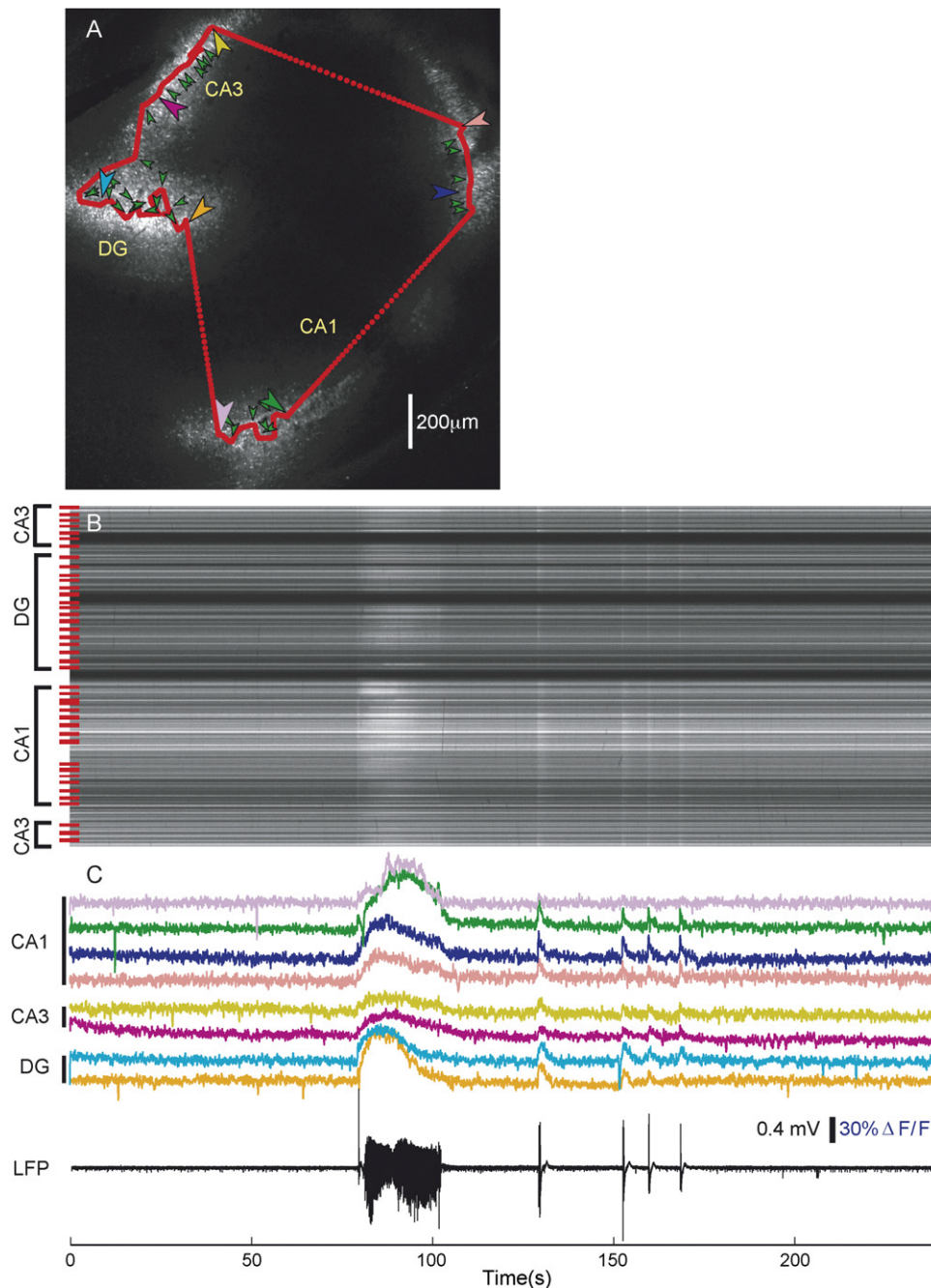


Fig. 3. Characterizing activity in many cells over a large distance. (A) Epileptiform activity was induced using 4-AP. Forty-one cells distributed over a region approximately $1600\ \mu\text{m} \times 1800\ \mu\text{m}$ ($10\times$ objective) were selected and imaged. (B) Scanning repeatedly along this path results in an image that records the calcium dynamics within cells as changes in brightness along rows. Red bars at the left of the image represent cells selected by the user. Bright rows without a corresponding red bar represent cells incidentally traversed between selected cells. Pixel rows falling within a cell can be grouped together and averaged to produce time traces of calcium activity for each cell. (C) The fluorescence signals from eight cells (B) are shown. LFP is the synchronously recorded local field potential acquired from CA3. Both seizure-like events and post-ictal bursting are apparent in this 4-min recording of both local field potential and in the imaged calcium signal. Fluorescence traces are low-pass filtered at 10 Hz. We emphasize that all the regions of the hippocampus CA1–CA3, as well as the dentate gyrus, have been encompassed here by a single scan path. The calcium dynamics recorded over a period of 4 min are illustrated in Supplemental Movie 1.

of the imaged cells (Fig. 3C, Supplemental Movie 1). The information in these traces was combined with the two-dimensional anatomical image to generate a movie of the network dynamics (see Supplemental Movies).

Using the same sampling densities described above, five cells distributed over a distance of $>1.1\ \text{mm}$ were monitored quasi simultaneously at a scan rate of 94.3 Hz (Fig. 4B, Supplemental Movie 2). To further verify that the measured calcium transients corresponded to action potentials in the recorded cells, one neuron was

whole-cell patch clamped and filled intracellularly with $10\ \mu\text{M}$ Calcium Green-1 (similar to the average pyramidal cell loading concentration obtained with multicell bolus loading (Stosiek et al., 2003)). The patched cell was scanned in a path that included 28 other neurons at a rate of 29.9 Hz. Action potentials elicited at random times with intracellular current pulses led to clearly observable relative fluorescence changes of $\sim 10\%$ (Fig. 4A). Even at this modest rate, action-potential-induced calcium transients were apparent in the unfiltered fluorescence trace (Fig. 4A, inset).

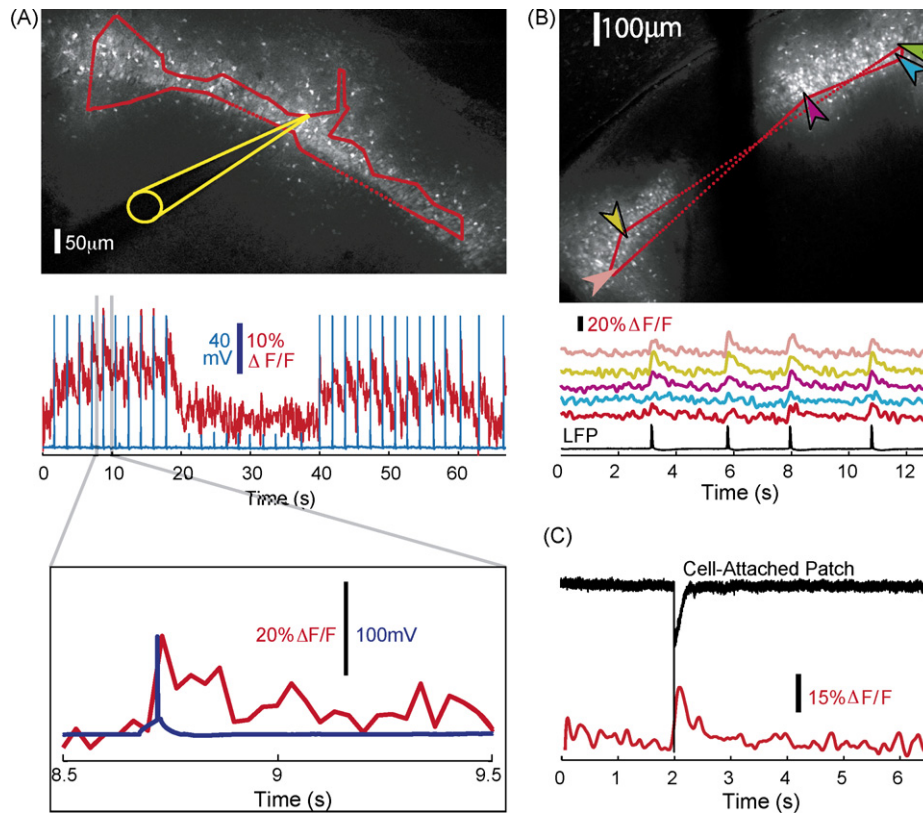


Fig. 4. Temporal resolution over a large distance. (A) The temporal and spatial resolutions are sufficient to resolve single action potentials (elicited by intracellular current injection) in a single cell (60× objective). The patch electrode filled with 10 μM Calcium Green-1 can be seen in the patched cell (electrode outlined in yellow). A combination of supra- and sub-threshold current pulses was applied to the patched cell. Inset shows the unfiltered calcium and membrane voltage traces for the one second surrounding an action potential. (B) Epileptiform activity (induced by 4-AP) was observed in five cells, in CA1, separated by a distance >1.1 mm at a rate of ~100 Hz (20× objective). The calcium dynamics recorded over a duration of 16 s are illustrated in Supplemental Movie 2. (C) To preserve the bulk-loaded dye concentration, a cell-attached patch voltage clamp recording was made during an extracellular stimulus. The action potential elicited is visible in both the optical and electrical signals (the stimulus artifact is deleted from the electrical trace). All fluorescence traces are low-pass filtered at 10 Hz.

Sub-threshold current pulses did not elicit obvious changes in fluorescence. To control for any possible difference in intracellular and bulk dye loading, a cell-attached patch recording was made. The electrode contained no calcium-sensitive dye to guarantee that no additional signal was introduced due to dye leaking across the membrane into the recorded cell. A 1-mA, 100-μs extracellular current pulse was used to elicit an action potential. The imaged calcium transient was synchronous with the electrical transient in the cell-attached patch recording and was comparable in amplitude to the whole-cell patch clamp example (Fig. 4C).

TPS could be used to record from an arbitrary number of neurons (as many as 41 are presented here). However, there is a tradeoff between the number of cells recorded N , the distance between cells l , the scan rate, and SNR. If the cells are assumed to be roughly uniformly distributed, then the roundtrip scan period (inverse scan rate) is given by

$$T = \sum_{i=1}^N \left(\Delta T + 2\sqrt{\frac{l_i}{\ddot{x}}} \right) \approx N\Delta T + 2\sqrt{\frac{NL}{\ddot{x}}} \quad (2)$$

where ΔT is the residence time per cell (samples per cell/sampling rate), L is the total path length, and \ddot{x} is the maximum acceleration. The SNR for a single cell measurement is proportional to $\sqrt{\Delta T}$. The principal benefit of using bang-bang control between cells is that the second term in Eq. (2) scales with \sqrt{NL} rather than NL .

The advantage of TPS over raster scanning increases with the average distance between recorded cells. To demonstrate this advantage, simulated scan paths were generated for cells (15-μm

diameter circles) separated by different distances. The scan paths were generated using both TPS (as described above) and homogeneously sampled raster-scanning strategies. For the raster scan, a pixel spacing was chosen to provide the same number of samples per cell as provided by TPS. That is, the SNR of both techniques was set to be the same. For purposes of comparison, we define cell density to be the percentage of pixels in the scan path that fall within cells of interest. Flyback time, which, in most implementations of raster scanning, is scan time wasted returning the mirror to the beginning of each row, was not considered here to provide a generous estimate of raster-scan cell density. Since TPS produces a closed path, it requires no flyback time. While the advantage of TPS is modest for closely spaced cells (Fig. 5A, 50 μm × 50 μm, 40 pixels per cell, TPS cell density = 38.6%, and raster cell density = 34.8%), the advantage grows dramatically when sampling cells that are sparsely distributed across a larger region (Fig. 5B, 200 μm × 200 μm, 40 pixels per cell, TPS cell density = 13.4%, and raster cell density = 1.6%). Increasing the number of pixels per cell to 100 improves the SNR by a factor of $\sqrt{1.4}$ and enhances the benefit of TPS even further (for 200 μm × 200 μm area, TPS cell density = 27.8%, raster cell density = 1.6%). The Supplemental materials include a Matlab script for comparing TPS and raster-scanning cell densities.

4. Discussion

We have described (and made available) a simple targeted-path strategy to constrain a laser scan path to user-defined SOI's and

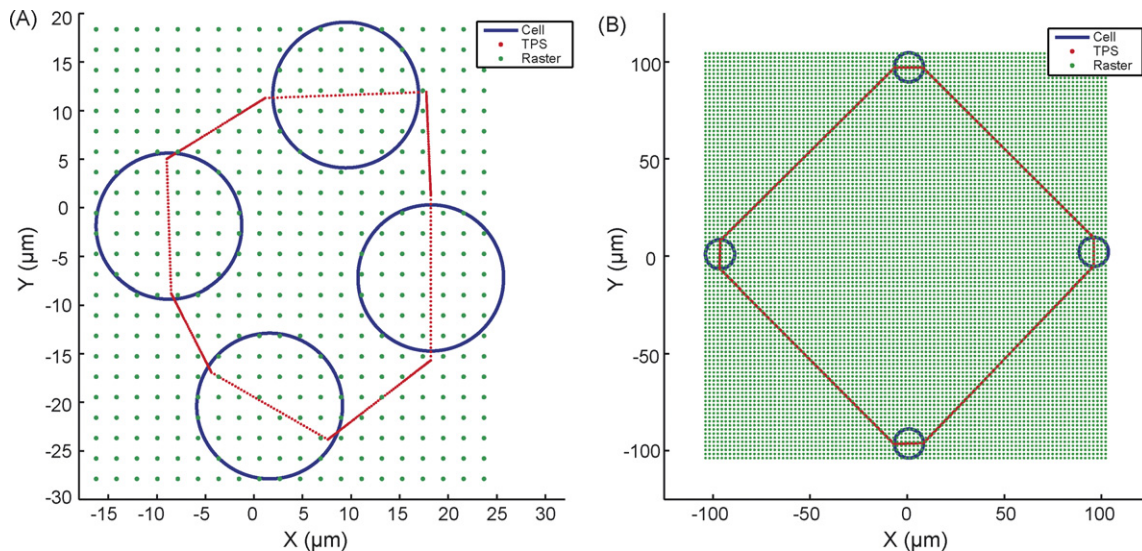


Fig. 5. TPS cell density. Cell density, defined here as the percentage of pixels in the scan path that fall within the boundaries of cells of interest, was determined using both TPS and raster scan-path generation strategies. Raster-scan pixel spacing was chosen to equal the number of pixels/cell achieved with TPS, yielding equivalent SNR for both techniques. (A) When cells are close together ($50\ \mu\text{m} \times 50\ \mu\text{m}$ region, 40 pixels per cell), TPS has a modest advantage in cell density (TPS cell density = 38.6%, raster cell density = 34.8%). (B) When cells are farther apart ($200\ \mu\text{m} \times 200\ \mu\text{m}$, 40 pixels per cell) TPS has a much greater advantage over raster scanning (TPS cell density = 13.4%, raster cell density = 1.6%).

minimize dead time between these SOI's. Because the laser travels at a constant speed through each region of interest, a well-defined SNR is essentially guaranteed for regions of the same approximate size and stain concentration.

We note that our experimental demonstrations made use of the relatively high-affinity Ca^{2+} -sensitive dye Calcium Green-1, which decays in brightness with a time constant of ~ 200 ms after an action potential. While scanning at a rate of 30 Hz with $\sim 400\ \mu\text{s}$ dwell time per cell was sufficient for detecting single action potentials, increasing scan rates and SNR would facilitate resolution of single action potential timing within bursts of action potentials. For single-spot scanning, scan speeds are inherently (shot noise) limited by the amount of time-per-cell (ΔT in Eq. (2)) required to achieve an acceptable SNR for a given application. Thus, there are two ways to increase scan rate: decrease ΔT (e.g. by increasing collection efficiency, fluorophore brightness, or fluorophore concentration) or increase acceleration between cells. The laser-spot acceleration between cells depends on the microscope objective used, maximum galvanometer torque (~ 900 dyne cm used here) and inertial load of mirror and rotor (0.03 gcm). Maximal single-spot scan speeds are always constrained by physical limits of galvanometers, detectors, and fluorophores. However, for a given system, TPS provides a framework to maximize the percentage of time spent scanning regions of interest without sacrificing spatial resolution or the ability to scan large FOV's deep in tissue.

Depending on cell selection, TPS could be used to image local networks, long-distance networks, or the interactions between them. For example, one could study how synchronization in CA3 networks affects interictal burst propagation through CA1 and subiculum. While examples shown in this paper focused on the study of networks of cells, TPS could be used to study neural activity at many scales. For example, dendritic integration could be examined by filling a single cell intracellularly and imaging dendritic branches (or even spines) as the regions of interest. Alternatively, TPS could also be used to photoactivate caged compounds at targeted regions within (e.g. caged calcium) or around (e.g. caged glutamate) the cell.

An advantage of beam steering with galvanometer-mounted mirrors is that it is hardware-compatible with standard two-photon

microscopes. Moreover, an enormous benefit of single-spot scanning is that the entire laser power is concentrated into a single focal point, providing a much more efficient generation of two-photon fluorescence than if the laser power were distributed over multiple focal points. When imaging deep within tissue, as is generally the goal in two-photon microscopy, a high two-photon excitation efficiency is indispensable (Helmchen and Denk, 2005). Finally, an advantage of using galvanometers over AOD's is that they are capable of much larger scan angles, and hence larger FOV's for a given objective. This is particularly important when using high N.A., low-magnification objectives that require significant beam expansion to accommodate their large apertures, and hence commensurately increased scan angles to maintain their full FOV. An important benefit of using low-magnification objectives is that, in addition to providing exceptionally wide FOV's, they also provide significantly enhanced fluorescence collection efficiency when imaging deep in tissue (Oheim et al., 2001), making them particularly appropriate for in vivo applications requiring single cell resolution over a large field of view.

The combined advantages of mirror-based scanning, minimized dead time, ease of implementation, and compatibility with high-resolution low-magnification objectives make targeted path scanning a particularly attractive approach for studying neuronal activity at many scales.

Acknowledgements

This work was partially funded by NIH grants EB005736, NS34425, MH61604, and the Burroughs Wellcome Fund 1001749.

Appendix A. Supplementary data

Supplementary data associated with this article can be found, in the online version, at doi:10.1016/j.jneumeth.2008.04.024.

References

Bewersdorf J, Pick R, Hell SW. Multifocal multiphoton microscopy. Opt Lett 1998;23:655–7.

- Chesnut TJ, Swann JW. Epileptiform activity induced by 4-aminopyridine in immature hippocampus. *Epilepsy Res* 1988;2:187–95.
- Fan CY, Fujisaki H, Miyawaki A, Tsay RK, Tsien RY, Ellisman MH. Video-rate scanning two-photon excitation fluorescence microscopy and ratio imaging with cameleons. *Biophys J* 1999;76:2412–20.
- Garaschuk O, Milos R-I, Konnerth A. Targeted bulk-loading of fluorescent indicators for two-photon brain imaging *in vivo*. *Nat Protoc* 2006;1:380–6.
- Göbel W, Kampa BM, Helmchen F. Imaging cellular network dynamics in three dimensions using fast 3D laser scanning. *Nat Methods* 2007;4:73–9.
- Helmchen F, Denk W. Deep tissue two-photon microscopy. *Nat Methods* 2005;2:932–40.
- Iyer V, Hoogland TM, Saggau P. Fast functional imaging of single neurons using random-access multiphoton (RAMP) microscopy. *J Neurophysiol* 2006;95:535–45.
- Kim KH, Buehler C, So PTC. High-speed, two-photon scanning microscope. *Appl Opt* 1999;38:6004–9.
- Kurtz R, Fricke M, Kalb J, Tinnefeld P, Sauer M. Application of multiline two-photon microscopy to functional *in vivo* imaging. *J Neurosci Methods* 2006;151:276–86.
- Lechleiter JD, Lin DT, Sieneart I. Multi-photon laser scanning microscopy using an acoustic optical deflector. *Biophys J* 2002;83:2292–9.
- Netoff TI, Banks MI, Dorval AD, Acker CD, Haas JS, Kopell N, White JA. Synchronization in hybrid neuronal networks of the hippocampal formation. *J Neurophysiol* 2005;93:1197–208.
- Nikolenko V, Poskanzer KE, Yuste R. Two-photon photostimulation and imaging of neural circuits. *Nat Methods* 2007;4:943–50.
- Oheim M, Beaupaire E, Chaigneau E, Mertz J, Charpak S. Two-photon microscopy in brain tissue: parameters influencing the imaging depth. *J Neurosci Methods* 2001;111:29–37.
- Perreault P, Avoli M. Effects of low concentrations of 4-aminopyridine on CA1 pyramidal cells of the hippocampus. *J Neurophysiol* 1989;61:953–70.
- Roorda RD, Hohl TM, Toledo-Crow R, Miesenbock G. Video-rate nonlinear microscopy of neuronal membrane dynamics with genetically encoded probes. *J Neurophysiol* 2004;92:609–21.
- Salomé R, Kremer Y, Dieudonné S, Léger JF, Krichevsky O, Wyart C, Chatenay D, Bourdieu L. Ultrafast random-access scanning in two-photon microscopy using acousto-optic deflectors. *J Neurosci Methods* 2006;154:161–74.
- Stosiek C, Garaschuk O, Holthoff K, Konnerth A. *In vivo* two-photon calcium imaging of neuronal networks. *Proc Natl Acad Sci USA* 2003;100:7319–24.
- Tan YP, Llano I, Hopt A, Wurriehausen F, Neher E. Fast scanning and efficient photodetection in a simple two-photon microscope. *J Neurosci Methods* 1999;92:123–35.
- Yi R, Chu KK, Mertz J. Graded-field microscopy with white light. *Opt Expr* 2006;14:5191–200.
- Zipfel WR, Williams RM, Webb WW. Nonlinear magic: multiphoton microscopy in the biosciences. *Nat Biotechnol* 2003;21:1369–77.